


# Assessing and enhancing foldability in designed proteins

Dina Listov<sup>1</sup> | Rosalie Lipsh-Sokolik<sup>1</sup> | Stéphane Rosset<sup>2</sup> | Che Yang<sup>2</sup> |  
Bruno E. Correia<sup>2</sup> | Sarel Jacob Fleishman<sup>1</sup> 

<sup>1</sup>Department of Biomolecular Sciences, Weizmann Institute of Science, Rehovot, Israel

<sup>2</sup>Institute of Bioengineering, École Polytechnique Fédérale de Lausanne (EPFL), Lausanne, Switzerland

## Correspondence

Sarel Jacob Fleishman, Department of Biomolecular Sciences, Weizmann Institute of Science, 7610001, Rehovot, Israel.  
Email: [sarel@weizmann.ac.il](mailto:sarel@weizmann.ac.il)

## Funding information

Ariane de Rothschild Women Doctoral Program; H2020 European Research Council, Grant/Award Numbers: 716058, 815379; Israel Science Foundation, Grant/Award Number: 1844/19; Schweizerischer Nationalfonds zur Förderung der Wissenschaftlichen Forschung, Grant/Award Number: 310030\_163139

**Review Editor:** Aitziber Cortajarena

## Abstract

Recent advances in protein-design methodology have led to a dramatic increase in reliability and scale. With these advances, dozens and even thousands of designed proteins are automatically generated and screened. Nevertheless, the success rate, particularly in design of functional proteins, is low and fundamental goals such as reliable de novo design of efficient enzymes remain beyond reach. Experimental analyses have consistently indicated that a major reason for design failure is inaccuracy and misfolding relative to the design conception. To address this challenge, we describe complementary methods to diagnose and ameliorate suboptimal regions in designed proteins: first, we develop a Rosetta atomistic computational mutation scanning approach to detect energetically suboptimal positions in designs (available on a web server <https://pSUFER.weizmann.ac.il>); second, we demonstrate that AlphaFold2 ab initio structure prediction flags regions that may misfold in designed enzymes and binders; and third, we focus FuncLib design calculations on suboptimal positions in a previously designed low-efficiency enzyme, improving its catalytic efficiency by 330-fold. Furthermore, applied to a de novo designed protein that exhibited limited stability, the same approach markedly improved stability and expressibility. Thus, foldability analysis and enhancement may dramatically increase the success rate in design of functional proteins.

## KEYWORDS

AlphaFold, computational design, FuncLib, protein folding, protein stability, pSUFER, Rosetta

## 1 | INTRODUCTION

Over the past decade, protein design methodology has made remarkable progress. New methods enable the routine design of new folds,<sup>1–4</sup> assemblies,<sup>5,6</sup> and new or improved functions.<sup>7–13</sup> Despite these achievements, however, only a small fraction of experimentally tested

designs are functional,<sup>8,14,15</sup> and fundamental protein design objectives still lie beyond our reach. For example, reliable de novo enzyme design remains an unsolved challenge despite decades of research, and to date, all designs exhibit low efficiency.<sup>15–17</sup> Previous analyses of successful and failed enzyme designs indicated that inaccuracies in the design of catalytic constellations are partly

This is an open access article under the terms of the [Creative Commons Attribution-NonCommercial](https://creativecommons.org/licenses/by-nc/4.0/) License, which permits use, distribution and reproduction in any medium, provided the original work is properly cited and is not used for commercial purposes.

© 2022 The Authors. *Protein Science* published by Wiley Periodicals LLC on behalf of The Protein Society.

to blame for failures.<sup>18–21</sup> Furthermore, observations across many different fold, binder, and enzyme design studies indicated misfolding relative to the design model as likely to be the most general and critical problem in failed designs.<sup>2,22–25</sup> Indeed, the significance of misfolding has served as the primary motivation for studies regarding the principles for designing new and idealized folds<sup>2,26,27</sup> and for developing general methods to improve designed proteins' foldability and stability.<sup>11,13,27–29</sup>

The current study is motivated by our ongoing efforts to develop a reliable strategy for de novo enzyme design. Our strategy is based on recent methods developed in our lab to design new backbones through the modular assembly of large (60–150 amino acid) backbone fragments of natural enzymes.<sup>25,30,31</sup> Modular assembly and design was successful in generating accurate antibodies<sup>27</sup> and ultrahigh specificity binders<sup>24</sup> and enzymes<sup>25</sup> with as many as 100 mutations from any natural protein. Applied to de novo enzyme design, however, this same strategy has so far failed to generate high-efficiency enzymes. Furthermore, the majority of the failed designs exhibited non-cooperative folding transitions. The correspondence between foldability and activity in our ongoing de novo enzyme design study prompts us to examine the sources of low foldability in proteins generated using current atomistic design methods and to develop strategies for detecting and ameliorating suboptimality in designed proteins.

## 2 | RESULTS

### 2.1 | Energy-based suboptimality detection

We develop an automated computational approach to identify energetically suboptimal positions in protein designs based on their model structure (Figure 1). Our approach, which we call pSUFER for protein Strain, Unsatisfactoriness, and Frustration finderER, starts by

relaxing the input structure using Rosetta atomistic modeling. It then models all single-point mutations at every position, iterating sidechain packing and whole-protein minimization and computes the change in system energy ( $\Delta\Delta G$ ) relative to the parental protein. These calculations use the Rosetta all-atom energy function 2015 (ref2015) which is dominated by van der Waals packing, hydrogen bonding, electrostatics, and implicit solvation.<sup>32</sup> Finally, pSUFER flags positions that exhibit more than a certain number of mutations (typically 5) that lower the native-state energy ( $\Delta\Delta G < 0$ ) as potentially suboptimal. These thresholds were chosen empirically and may be changed according to modeling needs. An online web server for automatically running pSUFER calculations is available for academic users at <https://pSUFER.weizmann.ac.il>. Customizable scripts for automatically relaxing a protein structure, computing suboptimal positions, and visualizing them in PyMOL are available in <https://github.com/Fleishman-Lab/pSUFER>.

Our approach is similar in principle to strategies for computing local frustration in proteins.<sup>33,34</sup> Methods for analyzing local frustration detect contacting pairs of amino acids that exhibit high energies relative to a computed ensemble of mutational or structural decoys. Frustrated positions are often associated with the protein's activity since active-site positions and regions that are involved in allosteric communication or conformational change are evolutionarily selected for their role in activity rather than for improving native-state stability.<sup>35</sup> We note, however, that since these previous approaches search for high-energy pairs of positions, they do not directly detect positions that may be optimized through single-point mutations. By contrast, pSUFER indicates specific positions for design.

### 2.2 | Orders of magnitude improvement in catalytic efficiency of a failed design

To test pSUFER, we analyzed a set of enzymes and binders designed and experimentally characterized over

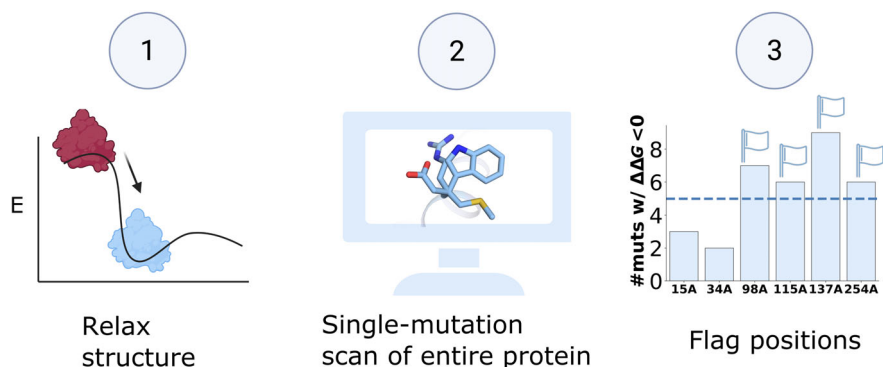


**FIGURE 1** Key steps in the pSUFER pipeline. (1) The structure is relaxed; (2) every position is mutated to every amino acid identity, the whole structure is relaxed and the energy is compared to the original relaxed structure; (3) positions that exhibit more stabilizing mutations than a predetermined threshold are flagged. pSUFER, protein Strain, Unsatisfactoriness, and Frustration finderER.

the past 4 years. To be included in this set, we required that the same design method produced both proteins that accurately folded into the design conception according to X-ray crystallography and ones that misfolded. Despite the availability of experimental structures in these cases, we applied pSUFER to the models to verify that the method could uncover flaws in the design conception without recourse to experimental data. The designs included enzymes<sup>25</sup> and binders<sup>24</sup> generated through modular backbone assembly and design as well as binders in which an immunogenic epitope was incorporated in a de novo designed scaffold protein.<sup>36</sup> Therefore, these designs encompass a range of contemporary applications of protein design methodology.

The first design pair we examine was generated by modular assembly and design of glycoside hydrolase 10 (GH10) xylanases.<sup>25</sup> In this set, 21 out of 43 designs exhibited detectable xylanase activity, and only two exhibited high activity levels as observed in natural enzymes from the GH10 family. From that study, we chose for pSUFER analysis two designs that exhibited the highest and lowest levels of detectable activity and for which we have crystallographic data, xyl3.1 and xyl8.3 ( $k_{\text{cat}}/K_M$  9,417 and  $0.61 \text{ M}^{-1} \text{ s}^{-1}$ , respectively). Both designs were highly mutated relative to natural GH10 enzymes, exhibiting 105 and 130 mutations from any natural enzyme, respectively (out of  $\sim 350$  amino acids) and exhibited apparent thermal denaturation temperatures  $>55^\circ\text{C}$ . The crystal structure of xyl3.1 showed remarkable accuracy relative to the design conception with  $0.7 \text{ \AA}$  root mean square deviation (rmsd) across the entire protein and  $<1 \text{ \AA}$  all-atom rmsd of active-site residues. By contrast, although xyl8.3 was globally accurate (rmsd =  $0.9 \text{ \AA}$ ) and core catalytic groups aligned well between the design model and the experimental structure, the experimental structure exhibited significant missing density in two neighboring loops near the active-site pocket, indicative of local misfolding. Visual inspection of the two designs following their structure determination failed to suggest significant flaws in xyl8.3 that might explain design inaccuracy.

Applied to the two xylanase design models, pSUFER flags a similar number of positions. As expected, most of the flagged positions are either in the active-site pocket or in solvent-accessible positions (Figure 2a,b). Conspicuously, however, in xyl8.3, pSUFER flags position Lys306, which is buried at the stem of one of the loops that does not exhibit electron density. Furthermore, Lys306 is not stabilized by counter charges, suggesting that the loop disorder may be the result of strain in and around this position.

We hypothesized that eliminating the strain observed around Lys306 (and the other positions flagged by

pSUFER) might improve the enzyme's catalytic efficiency. To test this hypothesis, we applied FuncLib design<sup>12</sup> to the five positions pSUFER flagged outside the active-site pocket in xyl8.3. FuncLib starts by using phylogenetic information and atomistic design calculations to rule out mutations that may be destabilizing to the native-state structure. It then enumerates all combinations of allowed mutations at the designed positions, ranks them by energy and suggests low-energy combinations of mutations. An advantage of the FuncLib methodology over typical stochastic combinatorial design algorithms is that FuncLib relaxes each combination of mutations by whole-protein minimization. Therefore, FuncLib may find stabilizing mutations, including radical small-to-large mutations in the core of the protein that may elude other atomistic design methods.<sup>37–39</sup> Applied to the five suboptimal positions flagged by pSUFER, one of the top FuncLib designs, which we called xyl8.3fix, improved system energy by 10 Rosetta energy units (R.e. u) by mutating four positions (Thr1Asn, Asn4Glu, Gly139Asp, and Lys306Leu). Among these four, only the Lys306Leu mutation is radical, whereas the others impact solvent-exposed positions to increase surface polarity.

We expressed xyl8.3 and xyl8.3fix fused N-terminally to maltose-binding protein (MBP) in *E. coli* BL21 cells and purified the proteins using an amylose column. We then tested the two designs' catalytic efficiency using the 4-nitrophenyl  $\beta$ -xylobioside (OPNPX2) chromogenic substrate. Remarkably, Michaelis–Menten analysis revealed that xyl8.3fix exhibits catalytic efficiency of  $226 \text{ M}^{-1} \text{ s}^{-1}$  (Figure 2c), 330-fold greater than that of the parental xyl8.3. We also analyzed the thermal denaturation of the two designs following cleavage from the MBP tag, finding that both had similar apparent denaturation temperatures  $57$  and  $59^\circ\text{C}$  for xyl8.3 and xyl8.3fix, respectively (Figure S1). Thus, the dramatic improvement in catalytic efficiency was not due to protein stabilization. Rather, it was likely due either to an improvement in the design's ability to fold into the active conformation or to reduced strain in the active site.

Significantly, in the modular assembly and design study that included xyl3.1 and xyl8.3,<sup>25</sup> we noted that assembling backbone fragments from more than a few natural templates led to low activity (xyl3.1 and 8.3 were based on 3 and 8 backbone fragments, respectively). The activity we observe for xyl8.3fix, however, would place it among the top three designs in that set despite comprising fragments from eight proteins. Thus, the pSUFER analysis may significantly improve the reliability of protein design methods and their ability to generate diverse and functional proteins.

To test whether a similar approach may improve computed system energies in other designs, we applied

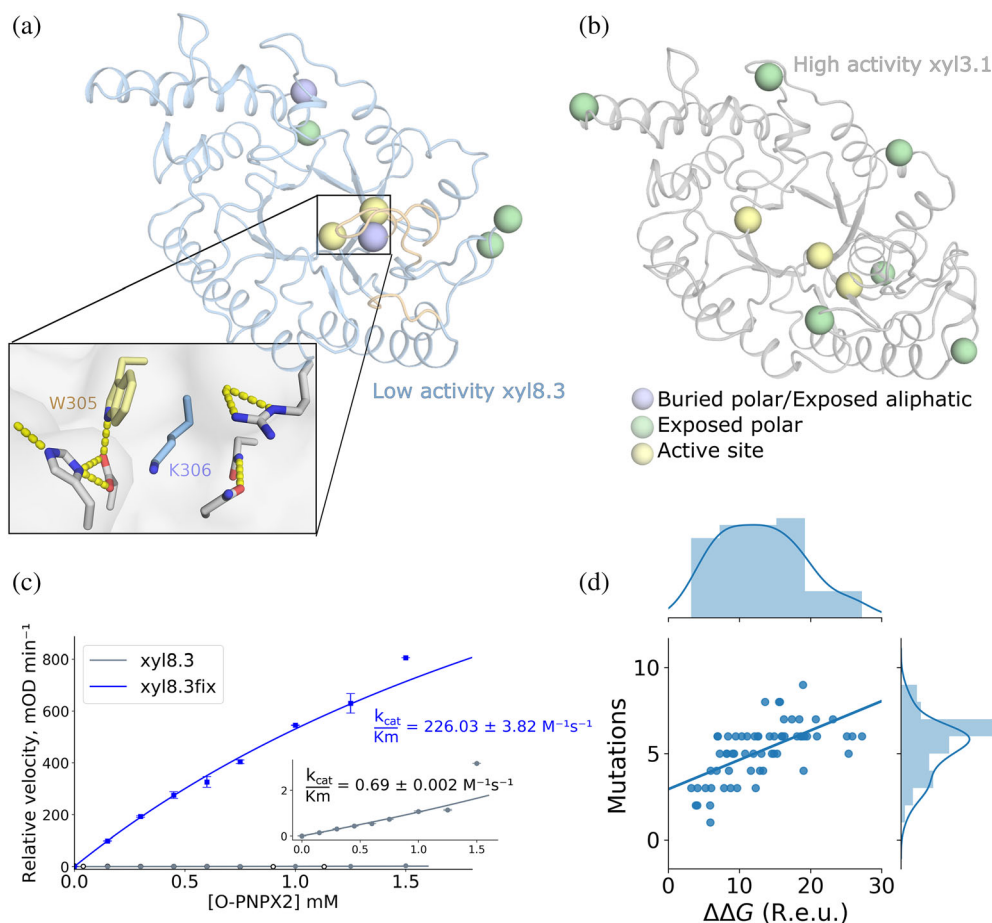


**FIGURE 2** pSUFER identifies flaws in enzyme designs that FuncLib can fix. (a) The xyl8.3 backbone is shown in cartoon with regions that failed to exhibit electron density in a crystallographic analysis (PDB entry: 6FHE) shown in wheat. (Inset) Lys306 is flagged by pSUFER since the Lys is buried in a hydrophobic region without countercharge stabilization. Lys306 is proximal to two loops that failed to exhibit electron density and is in close contact with active-site position Trp305. (b) For comparison, in the case of the high-efficiency and accurately designed xyl3.1, pSUFER only flags surface-exposed polar positions and active-site positions. In both cases, a position was flagged if computational mutation scanning suggested at least six amino acid identities with  $\Delta\Delta G < 0$  at the position. (c) xyl8.3fix shows an improvement of 330-fold in activity compared to xyl8.3,  $k_{\text{cat}}/K_{\text{M}} = 226$  and  $0.69 \text{ M}^{-1} \text{ s}^{-1}$ , respectively. Data points and standard deviations are based on at least two repetitions. (d) Improvement in system energy following FuncLib design of positions flagged by pSUFER in 62 models of de novo designed enzymes generated by modular assembly and design. On average, 5–6 mutations are introduced, yielding an average improvement of 13 Rosetta energy units (R.e.u.). pSUFER, protein Strain, Unsatisfactoriness, and Frustration finder.

FuncLib to positions flagged by pSUFER in 62 proteins designed in our lab to generate de novo enzymes. FuncLib introduced an average of five mutations and improved the energies by an average of 13 R.e.u. in this set (Figure 2d), similar to the values we obtained by applying this approach to xyl8.3. These computational results suggest that the pSUFER approach can be applicable to other significant challenges in protein design.

### 2.3 | Suboptimality in designed binders

We next ask whether pSUFER may shed light on problems in designed binders. In the following example, we

examine de novo designed binders of biosensors that detect and quantify epitope-specific antibodies. The design strategy uses a bottom-up approach: first defining the function-rendering motifs and then designing a protein fold to support the motifs.<sup>36</sup> One of the designs (4H.01) forms the binding site accurately as determined by X-ray crystallography; however, the experimentally determined structure shows substantial backbone deviations (2.9 Å) relative to the design conception and exhibits missing density in a loop (Figure 3a). pSUFER flags 11 positions in this design; for instance, Gln84, which is positioned in a cavity next to the loop that exhibits missing density, and Leu78. According to the design model, Gln84 is partly desolvated and does not



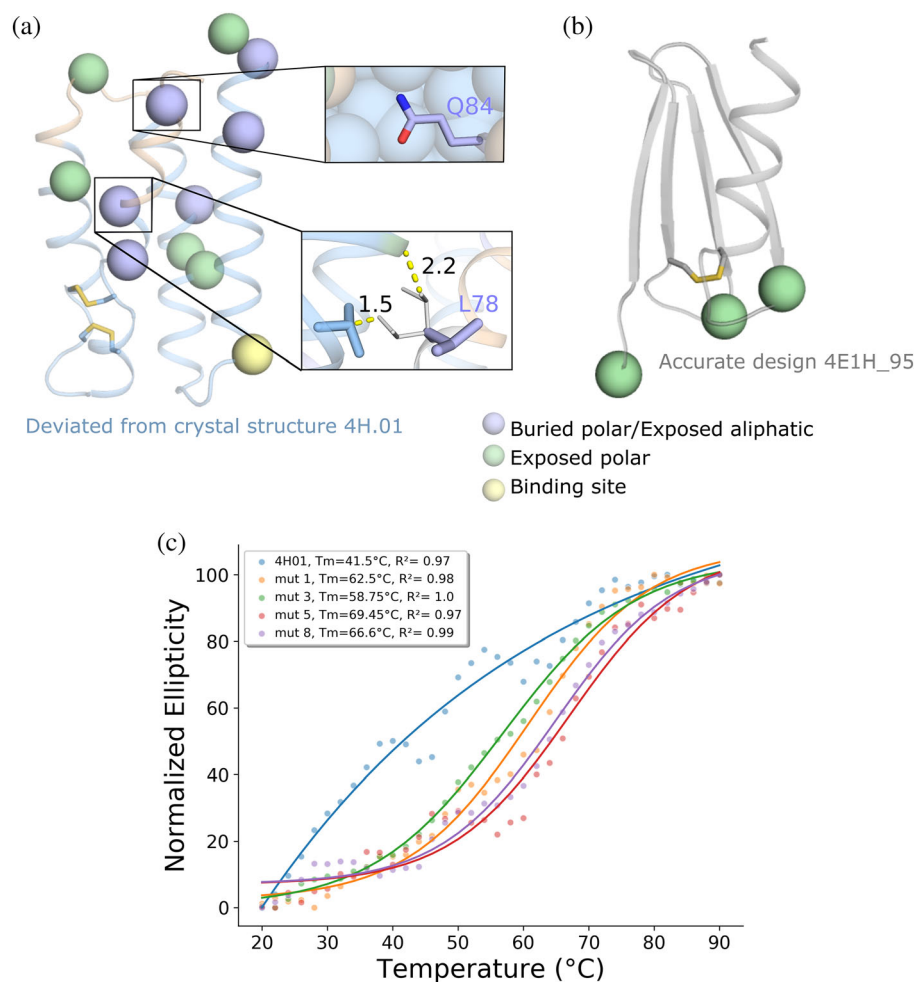


**FIGURE 3** pSUFER and FuncLib flag and improve the stability of a de novo designed binder. (a,b) pSUFER analysis of de novo designed binders. Positions were flagged if mutational scanning suggested at least four amino acid identities with  $\Delta\Delta G < 0$ . Wheat backbone marks missing density on the design model. Disulfides are indicated by sticks. (a) Crystallographic analysis of 4H.01 (PDB entry: 6YWD) revealed regions of missing density. pSUFER flags several strained positions in the design model surrounding the region that exhibited missing density. (thumbnails) Gln53 is partly desolvated but does not form stabilizing hydrogen bonds. The sidechain conformation of Leu78 is strained in the design model (purple). The most likely sidechain conformation for this position (white) is disallowed due to steric overlaps with neighboring sidechains. (b) Design 4E1H\_95 was atomically accurate as verified by X-ray crystallography (PDB entry: 6YWC) and pSUFER analysis flags only a few exposed polar sidechains. (c) Temperature melts of 4H01 variants monitored by CD at 220 nm. The original 4H.01 does not show cooperative melting curves as opposed to the FuncLib designs. pSUFER, protein Strain, Unsatisfactoriness, and Frustration findER

form intimate polar contacts with the loop. Leu78 is forced into a strained sidechain conformation exhibiting Rosetta sidechain conformation energy (fa\_dun) of  $\sim +3$  energy units. This sidechain cannot pack into a favorable conformation due to steric overlaps in relaxed sidechain conformations. In contrast to this design, in the accurately crystallized design, only three positions are flagged, all of which are solvent-exposed (His1, Thr19, and Thr35, Figure 3b).

We applied FuncLib to alleviate strain in the 4H.01 design. We chose eight flagged positions that were far from the binding site (His1, Met2, Glu7, His47, Gln53, Gly76, Leu78, and Gln84) for FuncLib design. As 4H.01

is a de novo design, phylogenetic analysis, which is a critical part of the FuncLib design strategy,<sup>12</sup> cannot be applied to it. Instead, we computed the free-energy change upon mutation for all 20 identities at each of the 11 strained positions, and mutations that exhibited  $\Delta\Delta G < +0.5$  R.e.u. were selected for full combinatorial enumeration and relaxation according to the FuncLib workflow. The lowest-energy 20 designs were visually inspected and 4 were chosen for experimental characterization. All designs harbored eight mutations compared to the original 4H.01, and at least two mutations compared to one another. In all designs, Gln84 was mutated to Leu, alleviating the desolvation penalty of the original Gln.

TABLE 1 Expressibility and stability of FuncLib variants of de novo designed 4H01

	Amino acid position								Expression levels ( $\mu\text{g/L}$ ) <sup>a</sup>	Tm ( $^{\circ}\text{C}$ ) <sup>b</sup>
	1	2	7	47	53	76	78	84		
4H01	H	M	E	H	Q	G	L	Q	54	41.4
4H01_mut1	P	E	T	T	K	R	A	L	128	62.4
4H01_mut3	P	E	T	S	K	R	S	L	146	58.7
4H01_mut5	P	E	D	R	K	R	A	L	108	68.4
4H01_mut8	P	E	T	R	K	S	A	L	78	66.6

<sup>a</sup>Determined using nanodrop.

<sup>b</sup>Determined by thermal melt analysis using circular dichroism (CD).

Furthermore, Leu78, which exhibited a strained side-chain conformation, was mutated to either Ala or Ser. The computed energies improved by at least 25 R.e.u.

The designs were expressed in pET11b vector, transformed into BL-21(DE3)pLySs cells, and the proteins were purified using HisTrap<sup>TM</sup> FF column following gel filtration on Superdex 16/600 75  $\mu\text{g}$ . All designs showed improvement of expression relative to 4H.01 of up to threefold. The designs also improved apparent thermal stability, as determined by circular dichroism, by 17–27 $^{\circ}\text{C}$  (Table 1, Figures 3c and S2). Moreover, the original 4H.01 design did not exhibit a clear melting transition, whereas all of the designs did. This suggests that the original 4H.01 design was not cooperatively folded and became a clearly folded protein upon the introduction of the eight designed mutations. We next attempted to test the designs' ability to bind their target antigen using surface plasmon resonance (SPR). The designs, however, exhibited high binding to the reference cell, precluding accurate affinity measurements and suggesting that they bind nonspecifically. Thus, the designed mutations substantially improved stability, expressibility, and apparent folding cooperativity but potentially at the price of loss in activity. Although it remains to be seen whether the FuncLib approach can be generally applied to de novo designed proteins, we conclude that the pSUFER strategy flags positions that are amenable to stabilizing mutations.

For a final example of pSUFER's abilities and limitations, we examine binders generated through modular assembly and design. Using modular assembly and design, we previously started from a high-affinity colicin endonuclease-immunity binding pair<sup>40</sup> to design a set of binders, some of which exhibited ultrahigh specificity (>100,000 fold) relative to the parental pair and other designed pairs.<sup>24</sup> Our approach focused on the design of a new interfacial loop backbone in the immunity protein by grafting loop backbones from completely unrelated proteins and optimizing the sequence of the binding pair. X-ray crystallographic analysis demonstrated that an

ultraspecific designed pair (des3) exhibited atomic accuracy throughout the structure and in the designed loop relative to the model, whereas a multispecific design (des4) exhibited missing density in parts of the designed loop.

We applied pSUFER to the immunity protein in the absence of its endonuclease partner. In each design, pSUFER flags a position within the designed binding loop (Figure 4a,b). The flagged position in des4, Gly26, cannot be redesigned as the backbone atoms of Gly26 come into close contact with the endonuclease. In des3, by contrast, two positions in the binding loop are flagged, Glu25 and Asn27. While Glu25 can be designed to other identities which are less strained according to our models, Asn27 forms polar contacts with the endonuclease and thus may be crucial for binding. In addition, in both designs pSUFER flags several solvent-accessible positions (Figure 4b). The results on des3 and des4 demonstrate that the pSUFER analysis may in some cases indicate problems that cannot be relieved without compromising the objectives of design of function.

## 2.4 | Analyzing design foldability by AlphaFold2

pSUFER analyzes suboptimality based on a molecular structure or model and is thus limited to analyzing the native-state properties of the design. Foldability, however, also depends on whether the protein is likely to fold into alternative (misfolded) states, a possibility that may be assessed by ab initio structure predictors. Recently, methods that use deep learning have been very successful in ab initio structure prediction.<sup>41–44</sup> The most successful of these, AlphaFold2, has shown atomic-accuracy prediction in community blind-prediction experiments and other structure-prediction challenges.<sup>41</sup> Significantly for the purposes of assessing design foldability, AlphaFold2 provides a confidence score (per-residue local distance

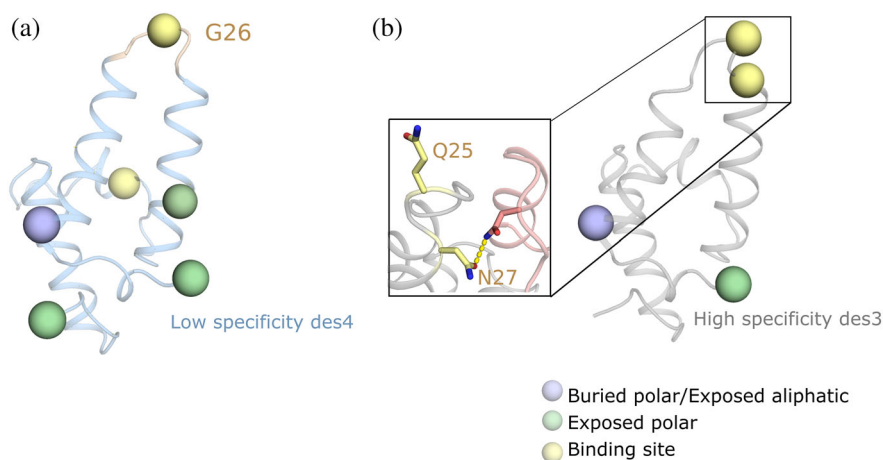


**FIGURE 4** pSUFER limitations in designed binders. (a,b) Binders generated through modular assembly and design by grafting an interfacial loop (top) from an unrelated protein and designing the two binding partners.<sup>24</sup> Positions were flagged if mutational scanning suggested at least six amino acid identities with  $\Delta\Delta G < 0$  at the position. Wheat backbone marks missing density on the design model. (a) The interfacial loop failed to exhibit electron density. pSUFER flags Gly26 in the designed loop. (b) pSUFER analysis of the accurately designed des3 flags exposed residues and two interfacial positions. Asn27 is one of the interface loop positions that forms polar contacts with the binding protein and thus may be crucial for function (inset). pSUFER, protein Strain, Unsatisfactoriness, and Frustration findER

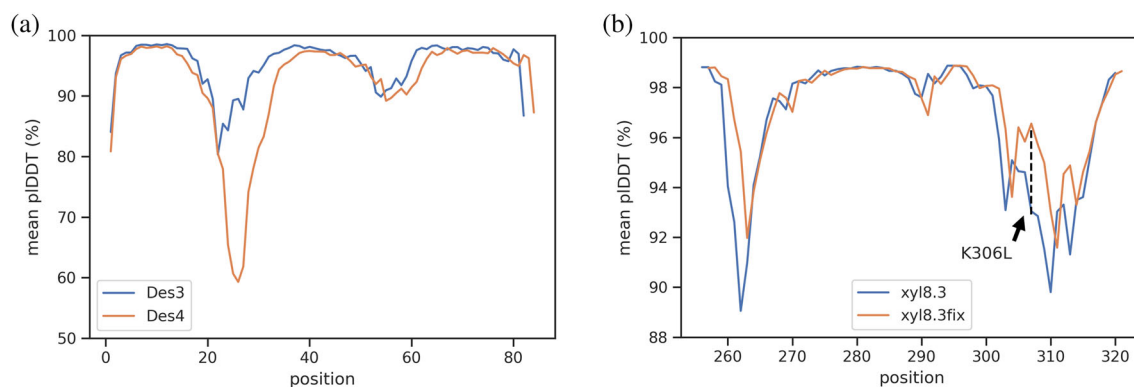


**FIGURE 5** AlphaFold2 analysis of designs. (a) pLDDT scores for designed binders des3 and des4. The pLDDT scores of des4 are depressed relative to those of des3 in the region in which des4 exhibits missing density. (b) Comparison of the pLDDT scores of xyl8.3 and design xyl8.3fix in the region surrounding the positions that exhibit missing density in crystallographic analysis of xyl8.3 (PDB entry: 6FHE; density is missing surrounding positions 259–265 and 301–312). In this region, only a single mutation was designed in xyl8.3fix, Lys306Leu; yet, the pLDDT scores of both loops improve significantly. pLDDT, per-residue local distance difference test

difference test; pLDDT) for each position in the predicted model structure. We hypothesized that the pLDDT scores and the rmsd between the AlphaFold2 predicted structure and the design model might predict design accuracy and foldability. AlphaFold2 depends on multiple-sequence alignments of homologs for accurate structure prediction so we did not analyze the de novo designed binders.

The AlphaFold2 analysis of the two accurately designed proteins (the GH10 xyl3.1 and the colicin immunity des3) correspond very well to the design models (rmsd  $< 0.7$  Å). Furthermore, except in the N- and C-terminal tails, the pLDDT scores are high in xyl3.1

and the majority of des3 ( $>90\%$ ). For des3, the binding-surface loop backbone was grafted from a non-homologous protein, explaining why the pLDDT scores are not as high in this region ( $>80\%$ ). Significantly, in the case of the colicin immunity des4, the AlphaFold2 model deviates from the design model in the region corresponding to the missing density (Figure 5a). Furthermore, the pLDDT scores clearly depress around these regions in both des3 and xyl8.3 relative to the two other designs. We next analyzed the AlphaFold2 results for xyl8.3fix. The AlphaFold2 model structure recapitulated the design model with rmsd  $< 0.8$  Å, similar to xyl8.3. Remarkably, the pLDDT scores in the region surrounding position

306, as well as in the loops that exhibit missing density according to the crystallographic analysis are higher and equivalent to those observed for the remainder of the protein (>92%) (Figure 5b). This result suggests that the AlphaFold2 confidence scores are sensitive even to some single-point mutations in designed proteins. We concluded that the AlphaFold2 analysis can provide critical information on the likely accuracy and foldability of newly designed backbone structures, indicate regions that may misfold, and assess mutations that are designed to mitigate misfolding.

### 3 | DISCUSSION

Recent advances in protein design methodology extend its scope to the design of large proteins that are highly mutated relative to natural ones<sup>25</sup> and to sets comprising thousands of designs.<sup>3,14</sup> Nevertheless, the success rate is typically low and some critical goals remain elusive. Thus, methods to assess design reliability may have a profound impact on the ability to design desired molecular activities. Assessing a design's accuracy and foldability, however, remains challenging. As a general rule, design studies, particularly ones devoted to backbone design, often reveal significant deviations between experimental structures and design conceptions. When the designs are small (<100 amino acids), they may be subjected to atomistic forward-folding *ab initio* simulations to verify that the sequences favor the designed conformation over others.<sup>1-3,45</sup> In large proteins, however, accurate forward-folding simulations were until recently impossible. Our results demonstrate that the deep-learning based method AlphaFold2 can shed light on design foldability even in large proteins that exhibit more than 100 mutations from any natural protein.

Furthermore, the pSUFER energy-based method can pinpoint specific positions that may be poorly designed. The functional consequences of poor design choices are strikingly demonstrated in our study: by redesigning just four positions in xyl8.3 that were flagged by pSUFER (out of 350 positions), and eight positions in 4H01 the enzyme's catalytic efficiency rises by three orders of magnitude, and the expressibility and stability of 4H01 improves by threefold and 27°C, respectively. These flagged positions are located outside the active or binding sites, demonstrating the significance of accurate and strain-free design throughout the protein. These observations, together with the improvement in the AlphaFold2 confidence scores for the enzyme design variant, implicate foldability or reduced active-site strain as the cause of improvement in activity. It is also striking that a

handful of poor design choices in a large protein led almost to complete dysfunction. We note, however, that the protein's ability to fold into the desired conformation also depends on other factors, such as the kinetic accessibility of the native state and the stability of folding intermediates.<sup>46</sup> These kinetic factors are not assessed by pSUFER, and it is unlikely that they can be deduced from current deep-learning-based *ab initio* structure predictors. Nevertheless, the strategy we described may free protein designers to introduce more radical changes than previously and increase the success of backbone design in large enzymes and binders.

### 4 | MATERIALS AND METHODS

#### 4.1 | pSUFER algorithm

RosettaScripts<sup>47</sup> and commandlines are available through github <https://github.com/Fleishman-Lab/pSUFER>. For all Rosetta calculations the ref15 energy function is used for scoring.<sup>48</sup> We start the procedure with four iterations of refinement of the input structure comprising sidechain packing and harmonically constrained whole-protein minimization. Next, computational mutation scanning is performed using the FilterScan mover in Rosetta<sup>10</sup>: for each position all 20 amino acids are modeled against the refined structure, and sidechains within 8 Å are repacked including constrained whole-protein minimization in order to accommodate the mutation. The energy difference between the refined structure and the single-point mutant is calculated. Positions that exhibit several mutations with  $\Delta\Delta G \leq 0$  R.e.u. are flagged as suboptimal with the mutation threshold in this work set to four for the *de novo* designed binders and six for all the other designs. Thresholds can be set by the user. pSUFER can be accessed through a web server at <https://pSUFER.weizmann.ac.il>. In this case, the user inputs a PDB-formatted coordinate file and the energy difference threshold for which a mutation is defined as favorable. The output consists of a folder containing (a) a PyMOL session file in which suboptimal positions are marked in yellow sticks. The session includes several models in which suboptimal positions are marked according to different cutoffs for the number of amino acid identities that exhibit  $\Delta\Delta G$  smaller than the set energy threshold. For instance, at threshold 4, all positions that exhibit 4 or more favorable identities relative to the starting structure are marked. (b) A table summarizing the suboptimal positions according to the cutoffs. (c) Tables indicating all of the favorable identities at each position (Rosetta resfile). (d) The Rosetta-refined structure.



## 4.2 | FuncLib design calculations

FuncLib on xyl8.3 was performed on the pSUFER flagged positions as described in<sup>12</sup> with the following thresholds  $PSSM \geq -2$  and  $\Delta\Delta G \leq 1$  R.e.u. in all flagged positions outside the active site. The 4H01 binder is the outcome of de novo design and lacks a multiple-sequence alignment from which a PSSM can be computed. We therefore extended the computational mutation scan to probe all 20 amino acid identities at any position  $>5$  Å from the binding site, and identities that exhibited  $\Delta\Delta G \leq 0.5$  R.e.u were chosen for combinatorial enumeration using FuncLib. All combinations of mutations were scored using Rosetta. For xyl8.3, within the top 20 designs ranked by system energy, the designs converged on the same solution for two of the positions and we chose the design that exhibited the most polar solvent facing residues (Thr1Asn and Asn4Glu) for experimental characterization.

## 4.3 | AlphaFold2 ab initio structure prediction calculations

All AlphaFold2<sup>41</sup> calculations were implemented by adapting and locally running the code written by ColabFold.<sup>49</sup> All runs were performed using the five model parameters presented in CASP14, without templates, with Amber relaxation and using three recycle rounds only. Multiple-sequence alignments were generated through the MMseqs2 API server.<sup>50–52</sup>

## 4.4 | Materials

4-Nitrophenyl  $\beta$ -xylobioside (OPNPX2) was purchased from Megazyme.

## 4.5 | Cloning, protein expression, and purification of xyl8.3

All experimental procedures were performed as described in Reference 25. Briefly, the xyl8.3fix design was ordered as a synthetic gene fragment from Twist Bioscience and cloned into pETMBPH vector which contains N-terminal 6-His-tag and MBP. EcoRI and PstI sites were used. The xyl8.3 and xyl8.3fix designs were transformed into BL21 DE3 cells and the DNA was extracted and validated by Sanger sequencing.

Fifty milliliters of 2YT with  $50 \mu\text{g ml}^{-1}$  kanamycin was inoculated with 500  $\mu\text{l}$  overnight culture and grown

at 37°C to OD of 0.4–0.8. Overexpression was induced by 0.2 mM isopropylthio- $\beta$ -galactoside and the cultures were grown for  $\sim 20$  hr at 20°C. Bacteria were pelleted by centrifugation and frozen for at least 20 min before purification.

Pellets were resuspended in lysis buffer (50 mM Tris-Cl pH 6.5, 150 mM NaCl, benzonase and  $0.1 \text{ mg ml}^{-1}$  lysozyme) and lysed by sonication. The supernatant was loaded on a column packed with amylose resin (New England Biolabs), washed twice with 50 mM Tris pH 6.5 and 150 mM NaCl, and eluted with wash buffer containing 10 mM maltose. Protein purity was evaluated by SDS-PAGE gel and protein concentration was estimated by OD<sub>280</sub>. In cases where purity was not satisfactory, the elution was loaded on an Ni-NTA, washed and eluted (50 mM Tris-Cl pH 6.5, 150 mM NaCl, 20 mM imidazole, and 250 mM imidazole, respectively). The proteins were then dialyzed against 50 mM Tris-Cl pH 6.5, 150 mM NaCl buffer.

## 4.6 | Kinetic measurements of xyl8.3

Kinetic measurements were performed with purified proteins (fused to MBP) in 96-well plates (optical length  $-0.5$  cm) by monitoring the absorbance of the leaving group of O-PNPX2 at 405 nm (activity buffer 50 mM Tris pH 6.5 and 150, 25°C). No background hydrolysis was observed with O-PNPX2. Final protein concentrations in the reaction varied between 2.56 and 6.23  $\mu\text{M}$ . The data were fitted to the linear regime of the Michaelis–Menten model ( $v_0 = [S]_0[E]_0 k_{\text{cat}}/K_M$ ) and  $k_{\text{cat}}/K_M$  values were deduced from the slope. The reported values represent the means  $\pm$  SD of at least two independent measurements.

## 4.7 | Apparent melting-temperature measurements of enzyme designs

$T_m$  measurements were done using nanoDSF experiments<sup>53</sup> performed on Prometheus NT.Plex instrument (NanoTemper Technologies). Melting temperatures were between 20 and 85°C with  $1.0^\circ\text{C min}^{-1}$  slope. For xyl8.3 and xyl8.3fix, the MBP tag was removed by tobacco etch virus cleavage. For xyl8.3 and xyl8.3fix, the buffer was 50 mM Tris-Cl pH 6.5, 150 mM NaCl. For de novo enzyme designs, the buffer was 100 mM Tris-Cl pH 7.25, 200 mM NaCl. Protein concentrations varied between 2.8 and 6.0  $\text{mg ml}^{-1}$  for all proteins. Fluorescence intensity was adjusted to suit all samples per experiment.

## 4.8 | Cloning, protein expression, and purification of 4H01 series

The 4H01 designs were ordered as a synthetic gene fragment from Twist Bioscience with addition of a C-terminal 6-His-Tag and cloned into a pET11b vector using NdeI and BpI restriction sites. The designs were transformed into XL-10-Gold cells and the DNA was extracted and validated by Sanger sequencing. The validated DNA sequences were transformed into BL21 DE3 cells and put in 20 ml of LB medium with 100  $\mu\text{g ml}^{-1}$  Ampicillin overnight at 37°C as starting cultures. The next day, 500 ml of Auto-Induction medium with 100  $\mu\text{g ml}^{-1}$  Ampicillin was inoculated with 10 ml overnight culture and grown at 37°C to OD of 0.6 then the cultures were grown for ~20 hr at 20°C. Bacteria were pelleted by centrifugation and resuspended in lysis buffer (100 mM Tris-Cl pH 7.5, 500 mM NaCl, 5% glycerol, 1 mM phenylmethanesulfonyl fluoride, 1 mg  $\text{ml}^{-1}$  lysozyme and 1:20 of CelLytic™ B Cell Lysis Reagent). The resuspensions were put at room temperature on a shaker at 40 rpm for 2 hr and then centrifuged at 48,300g for 20 min. We filtered the supernatant with a 0.2  $\mu\text{m}$  filter and loaded the mixture on a 1 mL His-Trap™ FF column using an AKTApure system and a predefined method regarding Cytiva's recommendations with that column. We used 50 mM Tris-HCl pH 7.5, 500 mM NaCl, 10 mM imidazole as wash buffer and processed the elution with 50 mM Tris-HCl pH 7.5, 500 mM NaCl, 500 mM imidazole. We collected the main fraction released through the elution step and injected it on a Gel Filtration column Superdex 16/600 75  $\mu\text{g}$  filled with PBS. The peaks corresponding to the size of the design were collected and concentrated till a concentration of ~1 mg  $\text{ml}^{-1}$  for further analysis. Protein concentrations were determined by nanodrop.

## 4.9 | Apparent melting-temperature measurements of 4H01 series

$T_m$  measurements were done using Chirascan™ V100 from appliedPhotophysics. Melting temperatures were between 20 and 90°C with measurements every 2°C.

### AUTHOR CONTRIBUTIONS

**Dina Listov:** Conceptualization (lead); data curation (lead); formal analysis (lead); investigation (lead); methodology (lead); software (lead); validation (lead); writing – original draft (lead); writing – review and editing (equal). **Rosalie Lipsh-Sokolik:** Data curation (supporting); formal analysis (supporting); investigation (supporting); methodology (supporting); validation (supporting).

**Stéphane Rosset:** Validation (supporting). **Che Yang:** Formal analysis (supporting). **Bruno Correia:** Formal analysis (supporting); funding acquisition (supporting); supervision (supporting); validation (supporting); writing – review and editing (supporting). **Sarel Jacob Fleishman:** Conceptualization (equal); funding acquisition (lead); investigation (equal); methodology (equal); project administration (lead); supervision (lead); validation (supporting); writing – original draft (equal); writing – review and editing (equal).

### ACKNOWLEDGMENTS

We thank Olga Khersonsky for help in xylanase activity screens and Ravit Netzer for advice in analyzing the colicin/endonuclease binders. Research in the Fleishman lab was supported by a Consolidator Award from the European Research Council (815379), an Individual Grant from the Israel Science Foundation (1844/19), the Dr. Barry Sherman Institute for Medicinal Chemistry, and a charitable donation in memory of Sam Switzer. Rosalie Lipsh-Sokolik is supported by a fellowship from the Arianne de Rothschild Women Doctoral Program. The Correia lab was supported by a Starting Grant from the European Research Council (716058) and a project grant from the Swiss National Science Foundation (310030\_163139).

### DATA AVAILABILITY STATEMENT

All relevant data is within the manuscript and its Supporting Information files.

### ORCID

Sarel Jacob Fleishman  <https://orcid.org/0000-0003-3177-7560>

### REFERENCES

1. Kuhlman B, Dantas G, Ireton GC, Varani G, Stoddard BL, Baker D. Design of a novel globular protein fold with atomic-level accuracy. *Science*. 2003;302:1364–1368.
2. Koga N, Tatsumi-Koga R, Liu G, et al. Principles for designing ideal protein structures. *Nature*. 2012;491:222–227.
3. Rocklin GJ, Chidyausiku TM, Goreshnik I, et al. Global analysis of protein folding using massively parallel design, synthesis, and testing. *Science*. 2017;357:168–175.
4. Jacobs TM, Williams B, Williams T, et al. Design of structurally distinct proteins using strategies inspired by evolution. *Science*. 2016;352:687–690.
5. King NP, Sheffler W, Sawaya MR, et al. Computational design of self-assembling protein nanomaterials with atomic level accuracy. *Science*. 2012;336:1171–1174.
6. Hsia Y, Bale JB, Gonen S, et al. Design of a hyperstable 60-subunit protein icosahedron. *Nature*. 2016;535:136–139.
7. Mou Y, Yu J-Y, Wannier TM, Guo C-L, Mayo SL. Computational design of co-assembling protein-DNA nanowires. *Nature*. 2015;525:230–233.

8. Fleishman SJ, Whitehead TA, Ekiert DC, et al. Computational design of proteins targeting the conserved stem region of influenza hemagglutinin. *Science*. 2011;332:816–821.
9. Chen K-YM, Keri D, Barth P. Computational design of G protein-coupled receptor allosteric signal transductions. *Nat Chem Biol*. 2020;16:77–86.
10. Whitehead TA, Chevalier A, Song Y, et al. Optimization of affinity, specificity and function of designed influenza inhibitors using deep sequencing. *Nat Biotechnol*. 2012;30:543–548.
11. Goldenzweig A, Goldsmith M, Hill SE, et al. Automated structure- and sequence-based design of proteins for high bacterial expression and stability. *Mol Cell*. 2018;70:380.
12. Khersonsky O, Lipsh R, Avizemer Z, et al. Automated design of efficient and functionally diverse enzyme repertoires. *Mol Cell*. 2018;72:178–186.e5.
13. Bednar D, Beerens K, Sebestova E, et al. FireProt: Energy- and evolution-based computational design of thermostable multiple-point mutants. *PLoS Comput Biol*. 2015;11:e1004556.
14. Chevalier A, Silva D-A, Rocklin GJ, et al. Massively parallel de novo protein design for targeted therapeutics. *Nature*. 2017; 550(7674):74–79. <https://doi.org/10.1038/nature23912>.
15. Röthlisberger D, Khersonsky O, Wollacott AM, et al. Kemp elimination catalysts by computational enzyme design. *Nature*. 2008;453:190–195.
16. Jiang L, Althoff EA, Clemente FR, et al. De novo computational design of retro-aldol enzymes. *Science*. 2008;319:1387–1391.
17. Privett HK, Kiss G, Lee TM, et al. Iterative approach to computational enzyme design. *Proc Natl Acad Sci U S A*. 2012;109: 3790–3795.
18. Baker D. An exciting but challenging road ahead for computational enzyme design. *Protein Sci*. 2010;19:1817–1819.
19. Sterner R. Faculty opinions recommendation of precision is essential for efficient catalysis in an evolved Kemp eliminase. Faculty Opinions—Post-Publication Peer Review of the Biomedical Literature [Internet]. 2013. <https://doi.org/10.3410/f.718146647.793485608>
20. Khare SD, Fleishman SJ. Emerging themes in the computational design of novel enzymes and protein-protein interfaces. *FEBS Lett*. 2013;587:1147–1154.
21. Korendovych IV, DeGrado WF. Catalytic efficiency of designed catalytic proteins. *Curr Opin Struct Biol*. 2014;27:113–121.
22. Khersonsky O, Kiss G, Röthlisberger D, et al. Bridging the gaps in design methodologies by evolutionary optimization of the stability and proficiency of designed Kemp eliminase KE59. *Proc Natl Acad Sci U S A*. 2012;109:10358–10363.
23. Fleishman SJ, Whitehead TA, Strauch EM, et al. Community-wide assessment of protein-interface modeling suggests improvements to design methodology. *J Mol Biol*. 2011;414:289–302.
24. Netzer R, Listov D, Lipsh R, et al. Ultrahigh specificity in a network of computationally designed protein-interaction pairs. *Nat Commun*. 2018;9(1):5286. <https://doi.org/10.1038/s41467-018-07722-9>.
25. Lapidoth G, Khersonsky O, Lipsh R, et al. Highly active enzymes by automated combinatorial backbone assembly and sequence design. *Nat Commun*. 2018;9:2780.
26. Dou J, Vorobieva AA, Sheffler W, et al. De novo design of a fluorescence-activating  $\beta$ -barrel. *Nature*. 2018;561:485–491.
27. Baran D, Pszolla MG, Lapidoth GD, et al. Principles for computational design of binding antibodies. *Proc Natl Acad Sci U S A*. 2017;114:10900–10905.
28. Goldenzweig A, Fleishman SJ. Principles of protein stability and their application in computational design. *Annu Rev Biochem*. 2018;87:105–129.
29. Weinstein J, Khersonsky O, Fleishman SJ. Practically useful protein-design methods combining phylogenetic and atomistic calculations. *Curr Opin Struct Biol*. 2020;63:58–64.
30. Lapidoth GD, Baran D, Pszolla GM, et al. AbDesign: An algorithm for combinatorial backbone design guided by natural conformations and sequences. *Proteins*. 2015;83:1385–1406.
31. Lipsh-Sokolik R, Listov D, Fleishman SJ. The AbDesign computational pipeline for modular backbone assembly and design of binders and enzymes. *Protein Sci*. 2021;30:151–159.
32. Park H, Bradley P, Greisen P Jr, et al. Simultaneous optimization of biomolecular energy functions on features from small molecules and macromolecules. *J Chem Theory Comput*. 2016; 12:6201–6212.
33. Ferreira DU, Komives EA, Wolynes PG. Frustration in biomolecules. *Q Rev Biophys*. 2014;47:285–363.
34. Ferreira DU, Komives EA, Wolynes PG. Frustration, function and folding. *Curr Opin Struct Biol*. 2018;48:68–73.
35. Freiburger MI, Guzovsky AB, Wolynes PG, Parra RG, Ferreira DU. Local frustration around enzyme active sites. *Proc Natl Acad Sci U S A*. 2019;116:4037–4043.
36. Yang C, Sesterhenn F, Bonet J, et al. Bottom-up de novo design of functional proteins with complex structural features. *Nat Chem Biol*. 2021;17:492–500.
37. VanDrisse CM, Lipsh-Sokolik R, Khersonsky O, Fleishman SJ, Newman DK. Computationally designed pyocyanin demethylase acts synergistically with tobramycin to kill recalcitrant *Pseudomonas aeruginosa* biofilms. *Proc Natl Acad Sci U S A*. 2021;118: e2022012118. <https://doi.org/10.1073/pnas.2022012118>.
38. Warszawski S, Borenstein Katz A, Lipsh R, et al. Optimizing antibody affinity and stability by the automated design of the variable light-heavy chain interfaces. *PLoS Comput Biol*. 2019; 15:e1007207.
39. Warszawski S, Netzer R, Tawfik DS, Fleishman SJ. A “fuzzy”-logic language for encoding multiple physical traits in biomolecules. *J Mol Biol*. 2014;426:4125–4138.
40. Cascales E, Buchanan SK, Duché D, et al. Colicin biology. *Microbiol Mol Biol Rev*. 2007;71(1):158–229. <http://mmb.asm.org/content/71/1/158.short>.
41. Jumper J, Evans R, Pritzel A, et al. Highly accurate protein structure prediction with AlphaFold. *Nature*. 2021;596:583–589. <https://doi.org/10.1038/s41586-021-03819-2>.
42. Baek M, DiMaio F, Anishchenko I, et al. Accurate prediction of protein structures and interactions using a three-track neural network. *Science*. 2021;373:871–876.
43. Wang S, Sun S, Li Z, Zhang R, Xu J. Accurate De novo prediction of protein contact map by ultra-deep learning model. *PLoS Comput Biol*. 2017;13:e1005324.
44. Evans R, O'Neill M, Pritzel A, et al. Protein complex prediction with AlphaFold-Multimer. *bioRxiv*. 2022;2021.10.04.463034. <https://doi.org/10.1101/2021.10.04.463034>.
45. Elazar A, Chandler NJ, Davey AS, et al. De novo-designed transmembrane domains tune engineered receptor functions. *Elife*. 2022;11:e75660.
46. Balchin D, Hayer-Hartl M, Hartl FU. In vivo aspects of protein folding and quality control. *Science*. 2016;353(6294):aac4354.

47. Fleishman SJ, Leaver-Fay A, Corn JE, et al. RosettaScripts: A scripting language interface to the Rosetta macromolecular modeling suite. *PLoS One*. 2011;6:e20161.
48. Alford RF, Leaver-Fay A, Jeliaskov JR, et al. The Rosetta all-atom energy function for macromolecular modeling and design. *J Chem Theory Comput*. 2017;13:3031–3048.
49. Mirdita M, Schuetze K, Moriwaki Y, Heo L, Ovchinnikov S, Steinegger M. ColabFold: making protein folding accessible to all. *Nat. Methods*. 2022;19(6):679–682.
50. Mirdita M, Steinegger M, Söding J. MMseqs2 desktop and local web server app for fast, interactive sequence searches. *Bioinformatics*. 2019;35:2856–2858.
51. Mirdita M, von den Driesch L, Galiez C, Martin MJ, Söding J, Steinegger M. Uniclust databases of clustered and deeply annotated protein sequences and alignments. *Nucleic Acids Res*. 2017;45:D170–D176.
52. Mitchell AL, Almeida A, Beracochea M, et al. MGnify: The microbiome analysis resource in 2020. *Nucleic Acids Res*. 2020;48:D570–D578.
53. Wedde S, Kleusch C, Bakonyi D, Gröger H. High-throughput feasible screening tool for determining enzyme stabilities against organic solvents directly from crude extracts. *Chembiochem*. 2017;18:2399–2403.

## SUPPORTING INFORMATION

Additional supporting information can be found online in the Supporting Information section at the end of this article.

**How to cite this article:** Listov D, Lipsh-Sokolik R, Rosset S, Yang C, Correia BE, Fleishman SJ. Assessing and enhancing foldability in designed proteins. *Protein Science*. 2022;31(9): e4400. <https://doi.org/10.1002/pro.4400>